Supplement of Atmos. Chem. Phys., 23, 9245–9263, 2023
https://doi.org/10.5194/acp-23-9245-2023-supplement

Atmospheric Chemistry and Physics
Open Access

Supplement of

Seasonal variations in the production of singlet oxygen and organic triplet excited states in aqueous $PM_{2.5}$ in Hong Kong SAR, South China

Yuting Lyu et al.

Correspondence to: Theodora Nah (theodora.nah@cityu.edu.hk)

Contents

List of Figures

List of Tables

1 S1. Detection of inorganic ions in $PM_{2.5}$ extracts

The main cations of sodium (Na^+), ammonium ($NH_4{}^+$), potassium (K^+), magnesium (Mg^{2+}), and calcium (Ca^{2+}), along with the main anions of fluoride (F^-), chloride (Cl^-), nitrate ($NO_3{}^+$), and sulfate ($SO_4{}^{2-}$) were detected using ion chromatography (IC) system (Dionex ICS-1100, Thermo Fisher Scientific). Separation of the cations was achieved using a Dionex IonPac CS12A analytical column (4 × 250 mm) equipped with a Dionex IonPac CG12A guard column (4 × 50 mm). Separation of the anions was achieved using a Dionex IonPac AS18 analytical column (4 × 250 mm) equipped with a Dionex IonPac AG18 guard column (4 × 50 mm) were used. 31 mM methanesulfonic acid (MSA) and 20 mM potassium hydroxide (KOH) were used as the eluents for the separations of cations and anions, respectively, and both were delivered at a flow rate of 1 mL min^{-1}.

2 S2. Determination of absolute spectral irradiance of 12 UVA lamps

An Ocean Optics USB-4000 UV-Vis spectrometer was used to record the relative spectral irradiance, and the photolysis rate of the chemical actinometer, 2-NB (10 µM), to quantify the absolute irradiance. The decay rates of 2-NB measured throughout this study were consistent ($0.0114 \pm 0.0002\ s^{-1}$), which indicated that the irradiance intensity of the light source was stable in the course of experiments. The absolute spectral irradiance ($I_{abs}(\lambda)$, mol-photons $cm^{-2}\ s^{-1}\ nm^{-1}$) was calculated using the following equation

$$I_{abs}(\lambda) = \gamma I_{rel}(\lambda) \tag{1}$$

where the relative irradiance $I_{rel}(\lambda)$ at each wavelength was recorded using a UV-Vis spectrometer (USB-4000, Ocean Optics), and the scaling factor γ was calculated using the following equation:

$$\gamma = \frac{k_{\text{2-NB}}}{\ln(10) \times (10^3\ \text{cm}^3\ \text{L}^{-1} \times 1\ \text{mol / N}_\text{A}\ \text{molecules}) \times \Sigma I_{rel}(\lambda) \times \delta\lambda \times \epsilon_{\text{2-NB}}(\lambda) \times \Phi_{\text{2-NB}}} \tag{2}$$

where $k_{2-\mathrm{NB}}$ is the first-order rate constant of 2-NB photolysis, ln(10) is the conversion factor from natural logarithms to common logarithms, $\delta\lambda$ is wavelength interval (1 nm), $\epsilon_{2-\mathrm{NB}}(\lambda)$ is the wavelength-dependent decadic molar absorptivity of 2-NB (Galbavy et al., 2010), and $\Phi_{2-\mathrm{NB}}$ is the wavelength-independent photolysis quantum yield (0.41) of 2-NB (Galbavy et al., 2010). The photolysis of 2-NB was monitored using ultra-high performance liquid chromatography (UPLC, Water ACQUITY H-Class) equipped with a photodiode-array detector (PDA) with a detection wavelength at 225 nm. Separation of 2-NB was performed using Kinetex Polar C18 column (2.6 μm, 100 × 2.6 mm) kept at room temperature.

3 S3. Seasonal trends in WSOC-normalized $[^1O_2^*]_{ss}$ and $[^3C^*]_{ss}$

We also normalized the $[^1O_2^*]_{ss}$ and $[^3C^*]_{ss}$ values determined for each extract by their WSOC concentrations and compared the resulting seasonal variations (Figures S14a and S14b) to the seasonal trends for the unnormalized $[^1O_2^*]_{ss}$ and $[^3C^*]_{ss}$ (Figures 4a and 4b). A similar, albeit weaker, seasonal trend for the normalized $[^1O_2^*]_{ss}$ (Figure S14a) was observed compared to the unnormalized $[^1O_2^*]_{ss}$ (Figure 4a). For both the normalized and unnormalized $[^1O_2^*]_{ss}$, the highest and lowest seasonal average values were obtained for winter and summer, respectively. The ratio of the average normalized $[^1O_2^*]_{ss}$ for winter vs. summer was 2.68, which was substantially smaller than the the ratio of the average unnormalized $[^1O_2^*]_{ss}$ for winter vs. summer (6.59). In the case of $^3C^*$, a weak (and statistically insignificant) seasonal trend was observed for the unnormalized $[^3C^*]_{ss}$, wherein the highest and lowest seasonal average values were obtained for winter and spring, respectively. The ratio of the average unnormalized $[^3C^*]_{ss}$ for winter vs. spring was 1.72 (Figure 4b), which was larger than the ratio of the average normalized $[^3C^*]_{ss}$ for winter vs. spring (0.89) (Figure S14b). Taken together, the weakened seasonal trends for the $[^1O_2^*]_{ss}$ and $[^3C^*]_{ss}$ values upon normalization to the WSOC concentrations underscored the key role that BrC chromophore quantity plays in driving $^1O_2^*$ and $^3C^*$ production in our study.

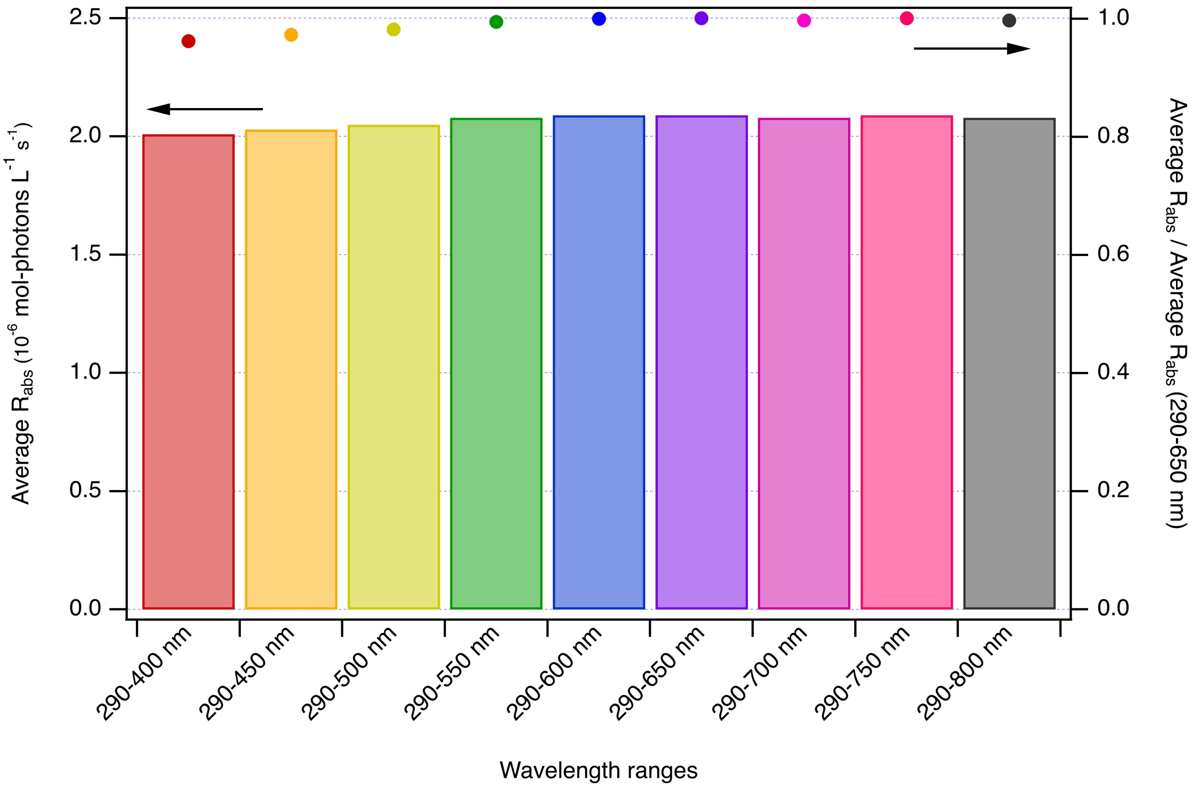

Figure S1. Comparison of the wavelength ranges for R_{abs} calculations for all the extracts. The right axis shows the percentages of R_{abs} integrated over a specific wavelength range with reference to R_{abs} integrated over the wavelength range of 290-600 nm.

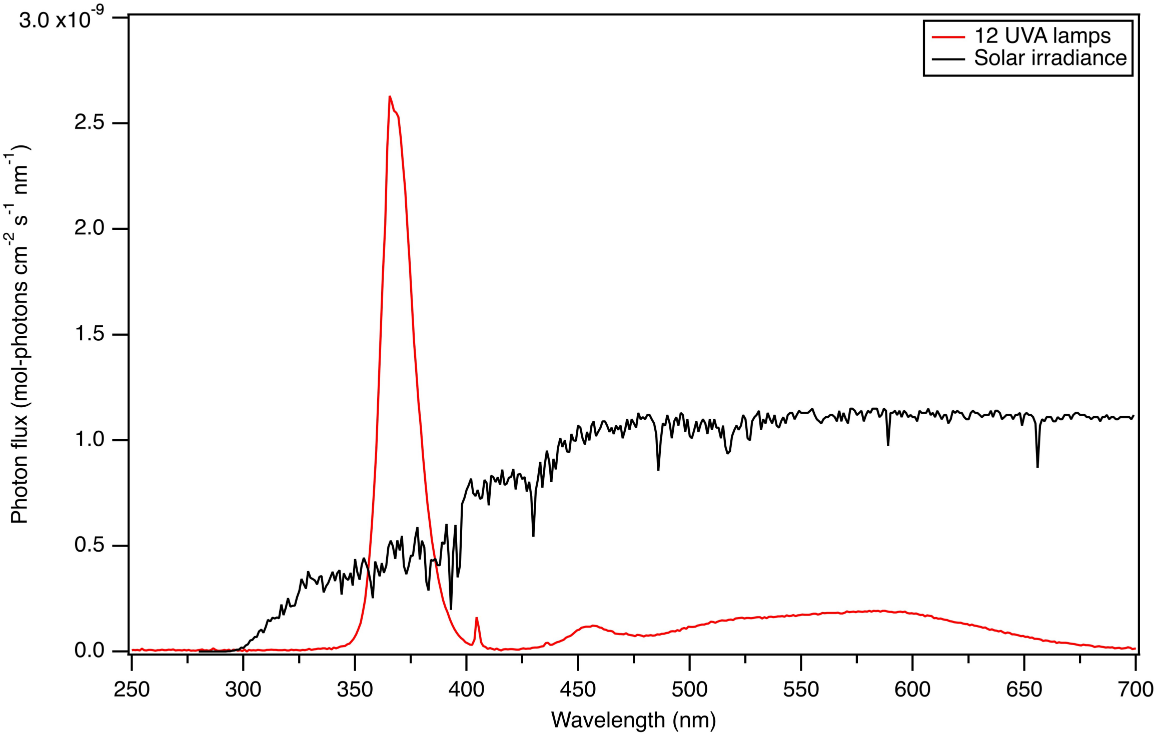

Figure S2. Absolute irradiance of 12 UVA lamps used in photochemical experiments, and comparison with solar irradiance at Hong Kong on summer solstice at noon (21/06/2021).

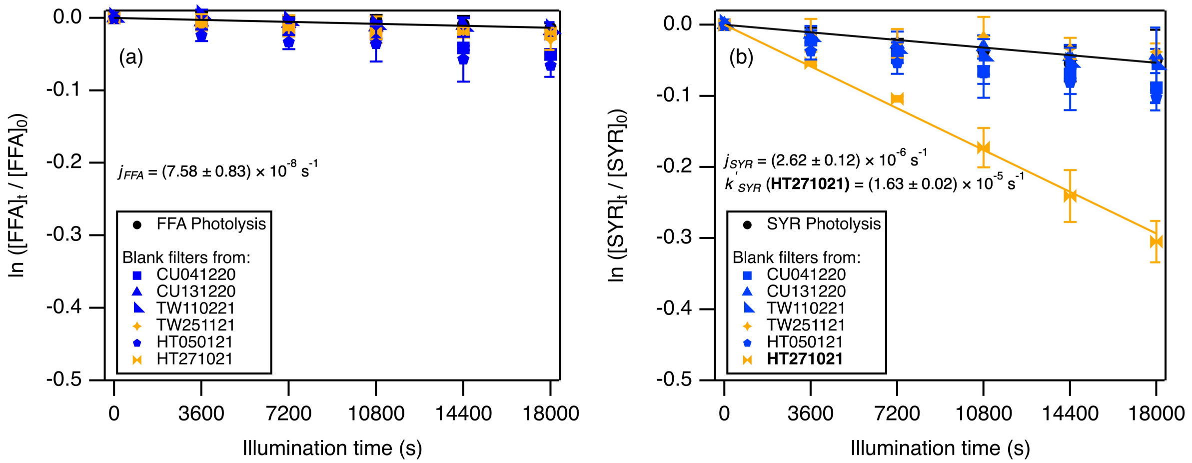

Figure S3. Loss of FFA and SYR in the extracts of six field blank filters collected concurrently with corresponding $PM_{2.5}$ filters during fall and winter seasons. Error bars indicate one standard deviation from triplicate experiments performed on different days. Although SYR showed obvious degradation in the extract of the HT271021 blank filter, the decay rate constant (k'_{SYR}) comprised a small fraction (less than 5 %) of the measured decay rate constants for the extracts of the corresponding $PM_{2.5}$ sample (Figures S4 and S5).

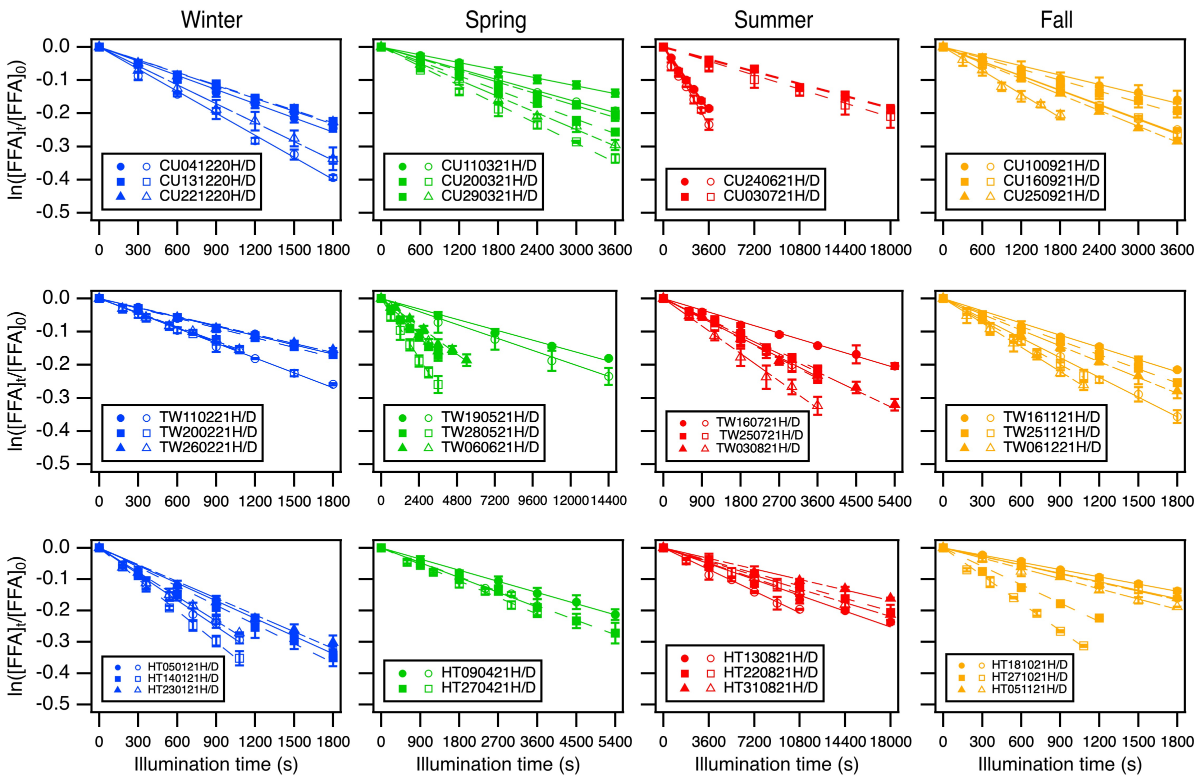

Figure S4. Pseudo first-order degradation kinetics of FFA in pure H_2O (filled symbols) and 1:1 H_2O/D_2O (empty symbols) experiments for the extracts. Blue, green, red, and orange symbols denote the winter, spring, summer, and fall samples. Error bars indicate one standard deviation from triplicate experiments performed on different days.

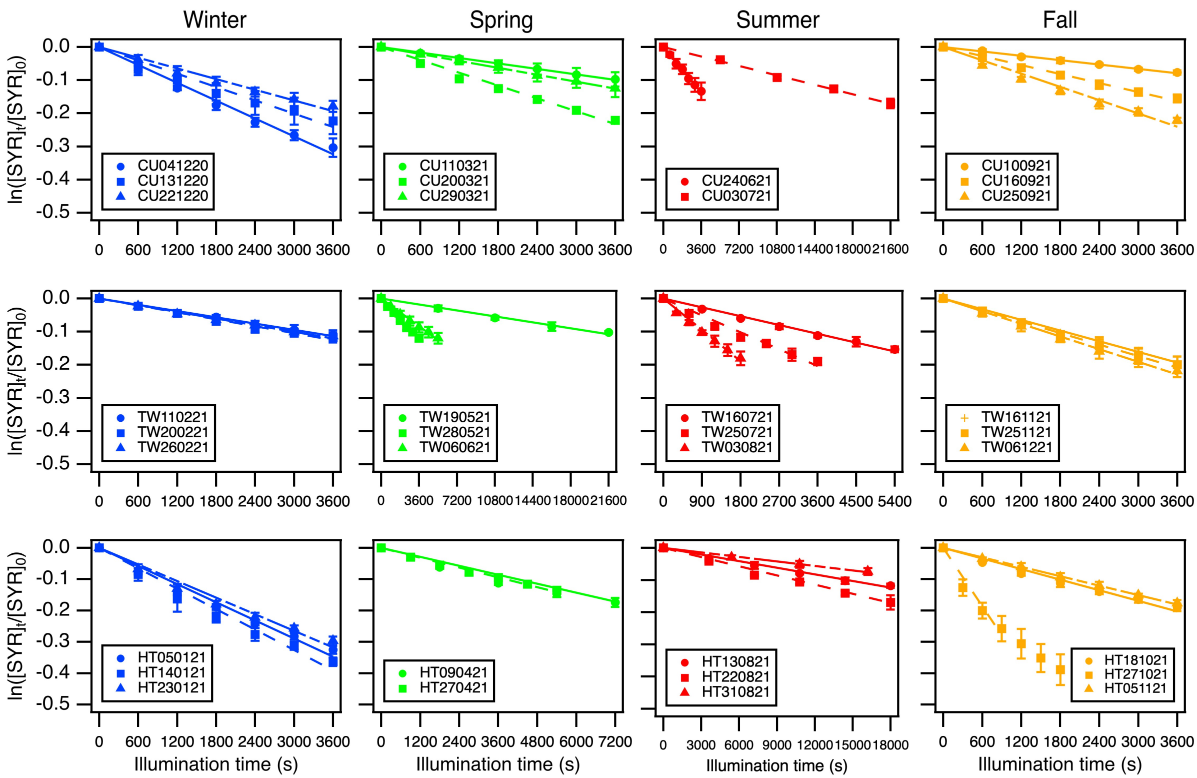

Figure S5. Pseudo first-order degradation kinetics of SYR in photochemical experiments for the extracts. Blue, green, red, and orange symbols denote the winter, spring, summer, and fall samples. Error bars indicated one standard deviation from triplicate experiments performed on different days. Initial fit was applied to sample HT271021 due to photobleaching.

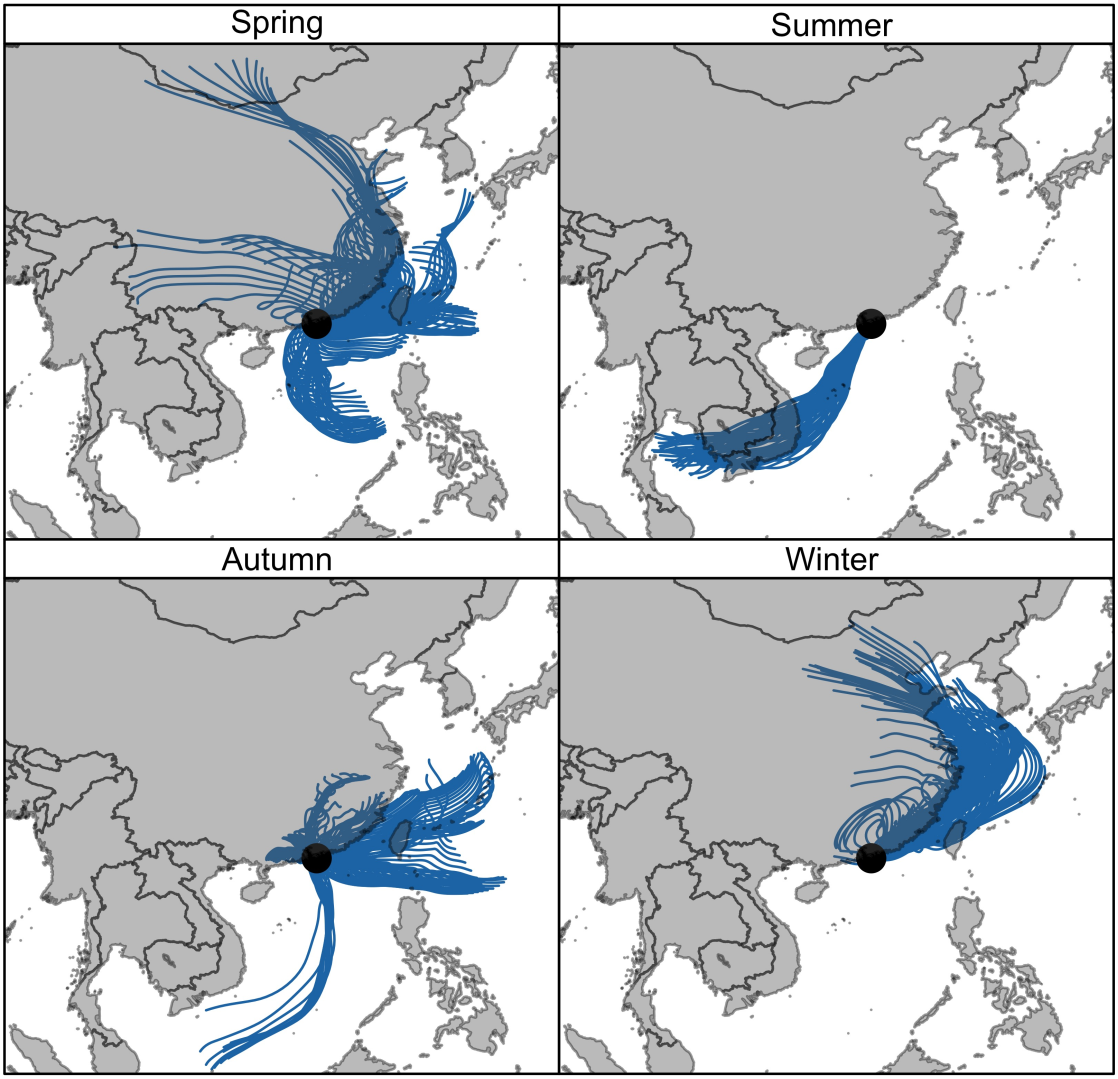

Figure S6. The 72-h backward trajectories arriving at CU (22°20’05”N, 114°10’23”E) at an elevation of 500 m.

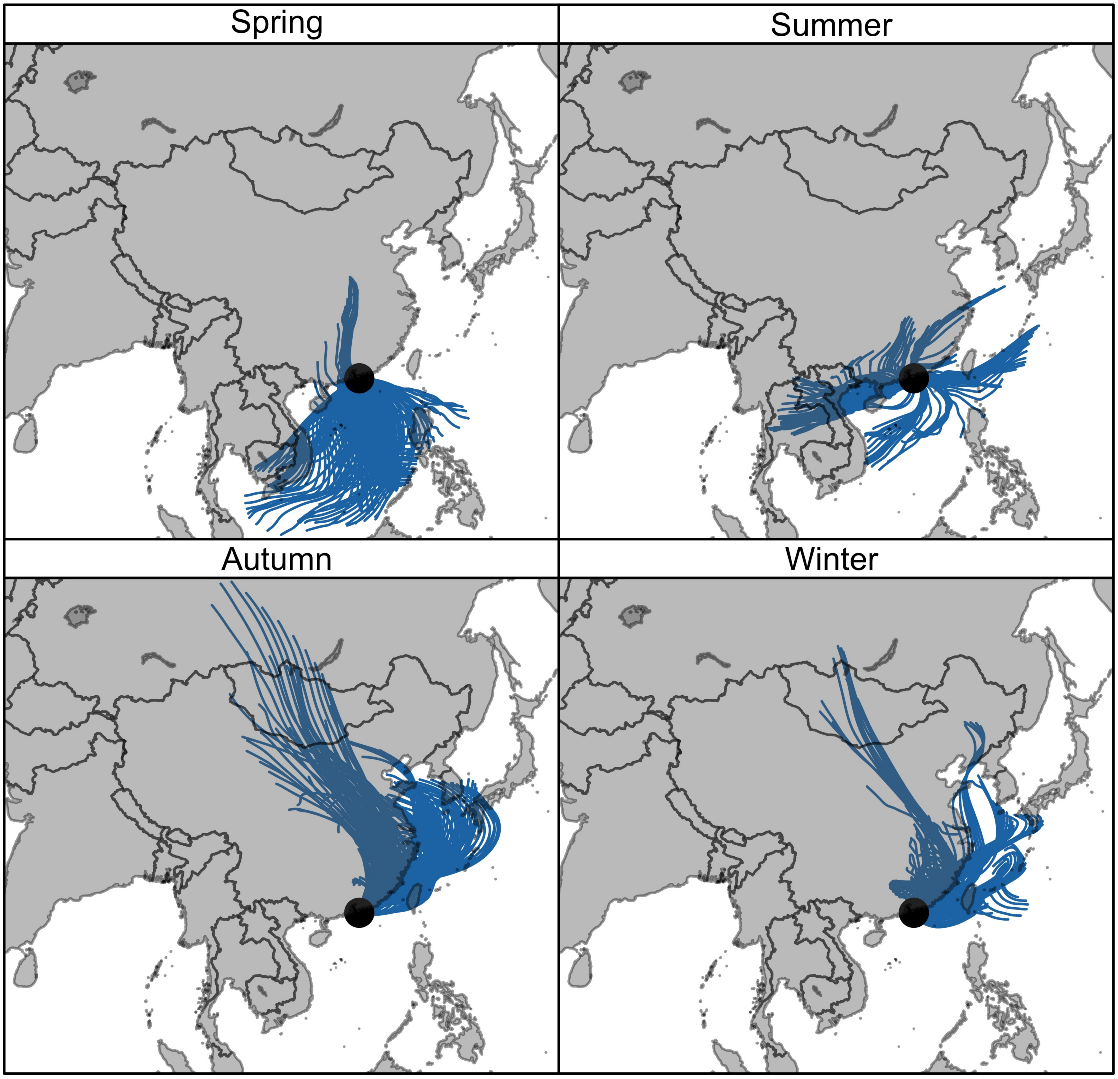

Figure S7. The 72-h backward trajectories arriving at TW (22°20'17"N, 114°06'52"E) at an elevation of 500 m.

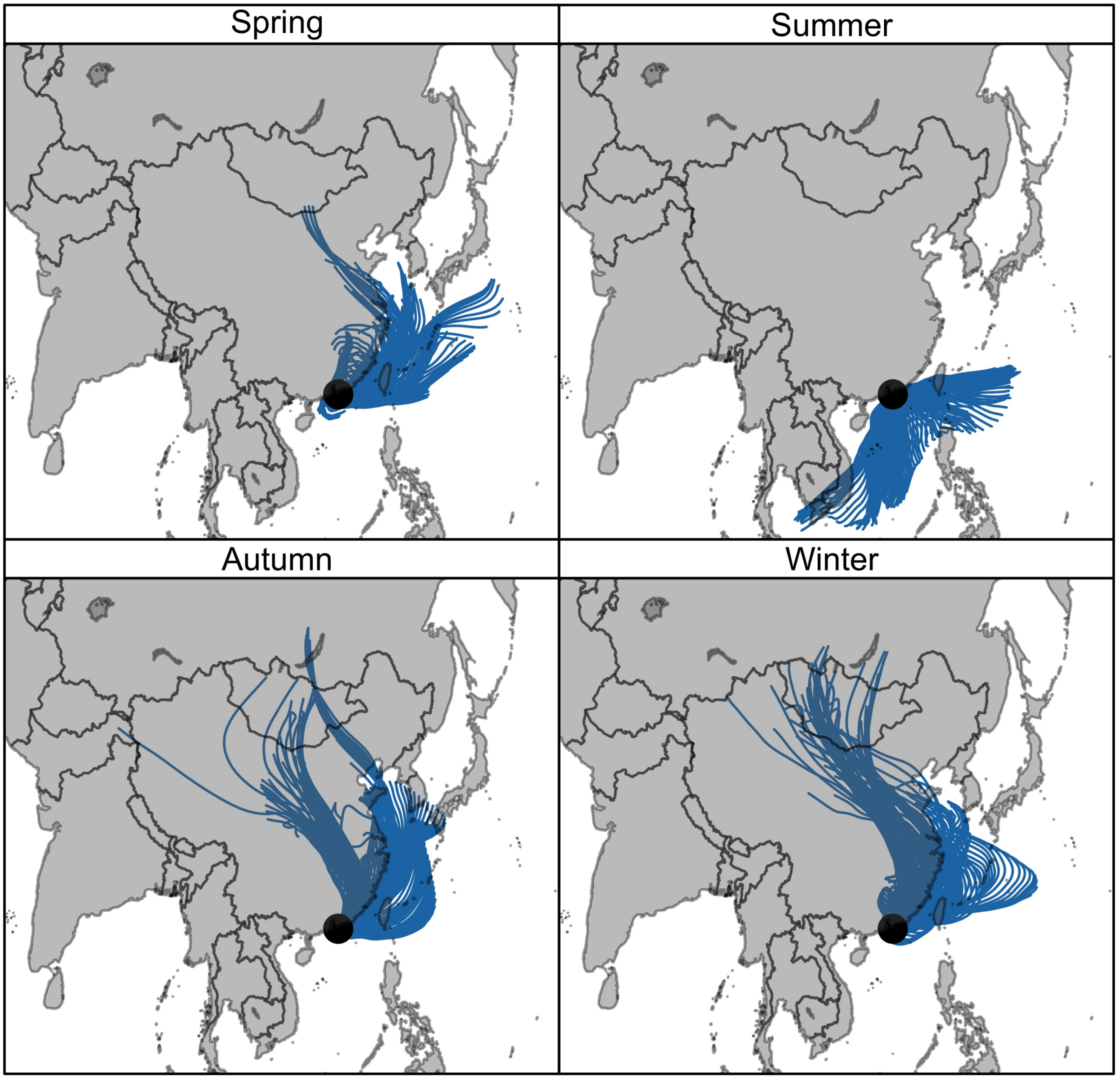

Figure S8. The 72-h backward trajectories arriving at HT (22°12’33”N,114°15’12”E) at an elevation of 500 m.

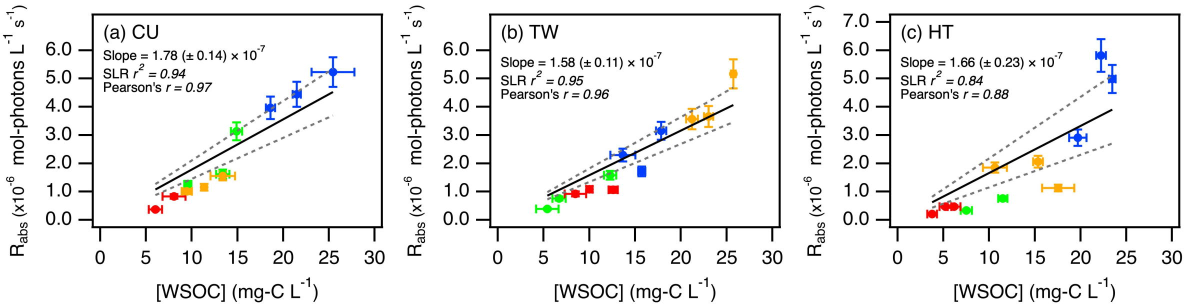

Figure S9. Correlation plots of the light absorption rates (R_{abs}) and the WSOC concentrations ([WSOC]) for CU, TW, and HT extracts, respectively. Blue, green, red, and orange symbols denote the winter, spring, summer, and fall samples. Dashed lines represent 95 % confidence bands. SLR r^2 and Pearson's r are the coefficient of determination of simple linear regression and Pearson correlation coefficient, respectively.

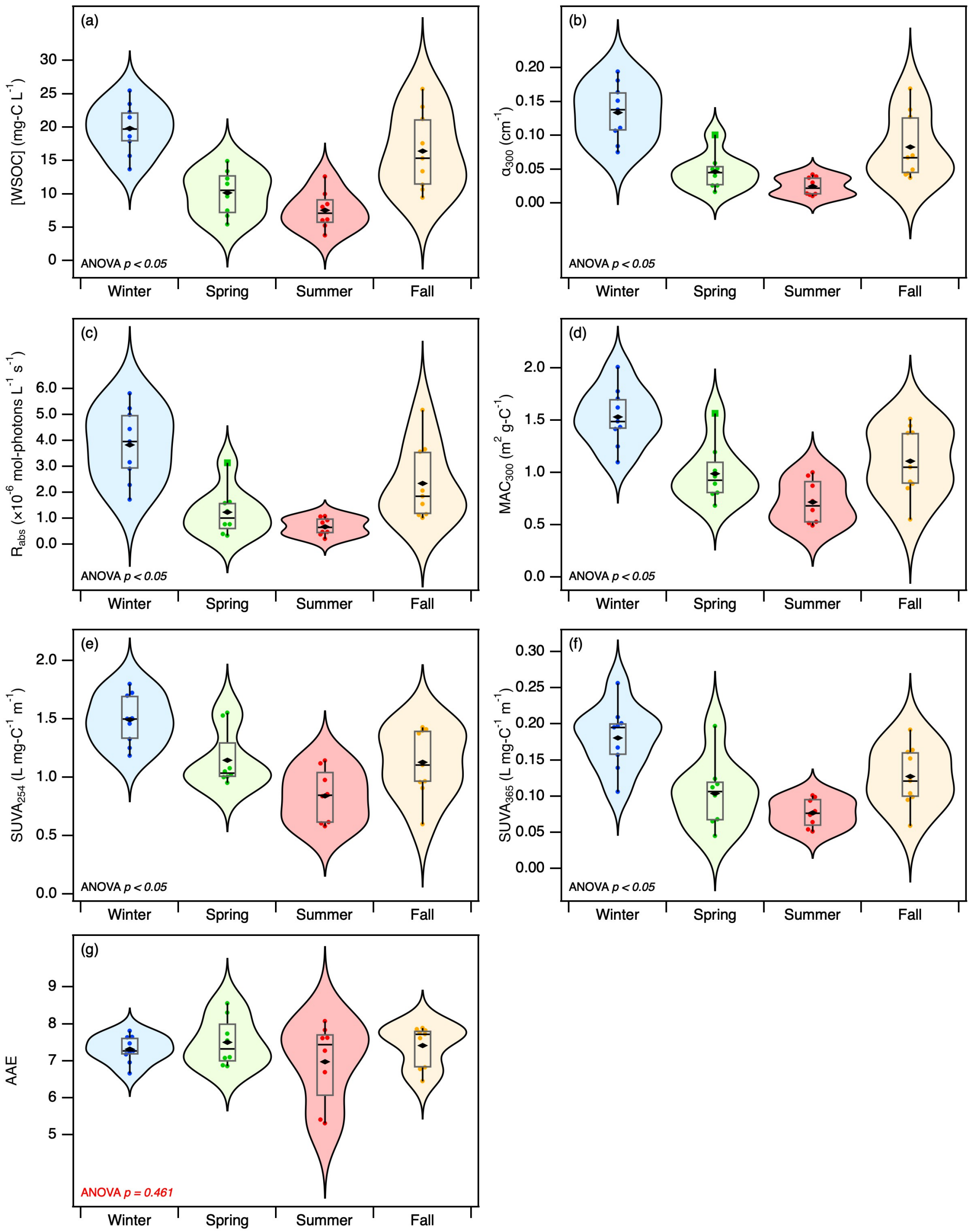

Figure S10. Violin plots showing the seasonal variations of light absorption properties for the extracts. For the box plots, the squares indicate outliers identified by Tukey's fences, the whiskers denote the minimum and maximum values, the boxes denote the 25^{th} and 75^{th} percentile values, black diamonds indicate the mean values, and the boxes' midline denote the median values.

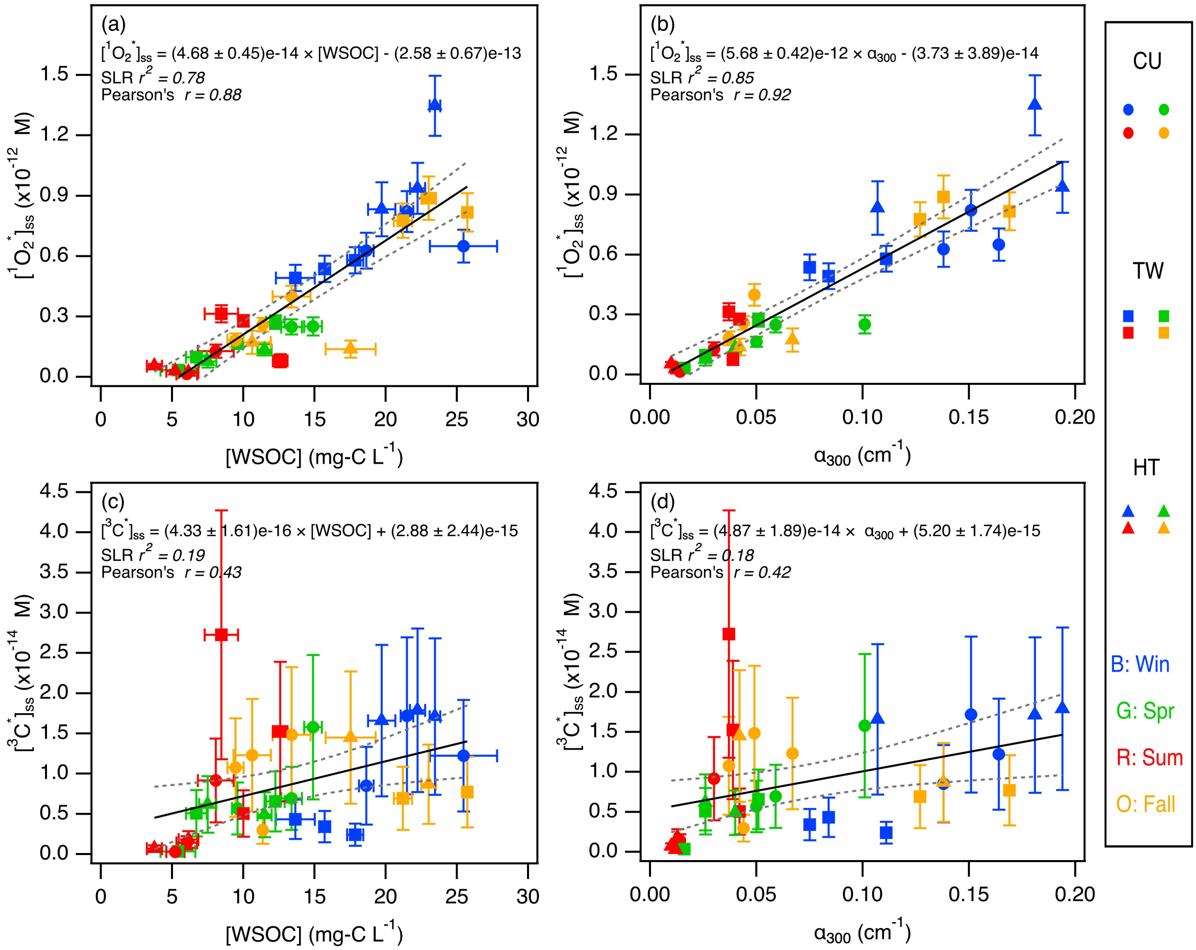

Figure S11. (a and b) $[^1O_2^*]_{ss}$ and (c and d) $[^3C^*]_{ss}$ as a function of WSOC concentration and α_{300}. The outlier (HT271021) was excluded. Blue, green, red, and orange symbols denote the winter, spring, summer, and fall samples, respectively. Dashed lines represent 95 % confidence bands. SLR r^2 and Pearson's r are the coefficient of determination of simple linear regression and Pearson correlation coefficient, respectively.

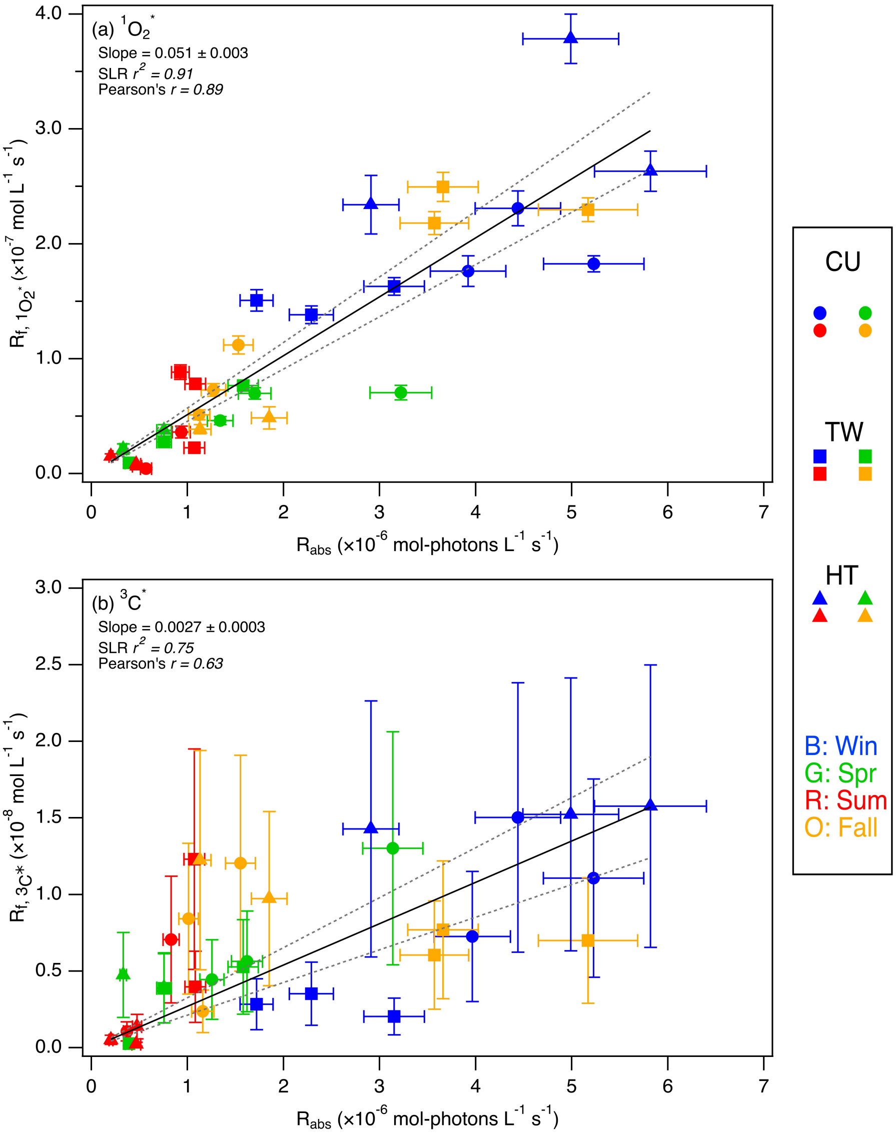

Figure S12. (a) $R_{f,{}^1O_2^*}$ and (b) $R_{f,{}^3C^*}$ as a function of R_{abs} for all three sites. The outlier (HT271021) was excluded. Blue, green, red, and orange symbols denote the winter, spring, summer, and fall samples, respectively. Dashed lines represent 95 % confidence bands. SLR r^2 and Pearson's r are the coefficient of determination of simple linear regression and Pearson correlation coefficient, respectively.

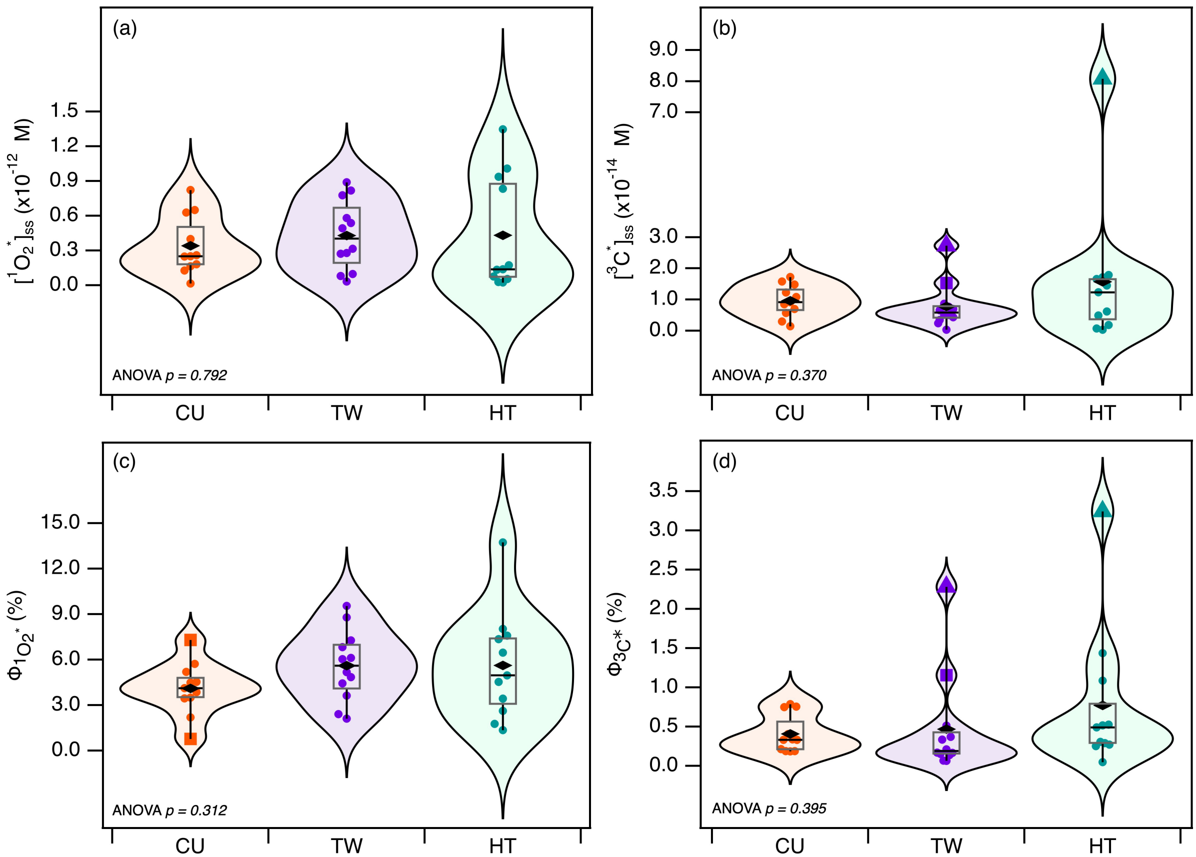

Figure S13. Violin plots showing the site variations of (a) $[^1O_2^*]_{ss}$, (b) $[^3C^*]_{ss}$, (c) $\Phi_{^1O_2^*}$, and (d) $\Phi_{^3C^*}$. For the box plots, the triangles indicate "far-out outliers" and the squares indicate outliers identified by Tukey's fences, the whiskers denote the minimum and maximum values, the boxes denote the 25th and 75th percentile values, black diamonds indicate the mean values, and the boxes' midline denote the median values.

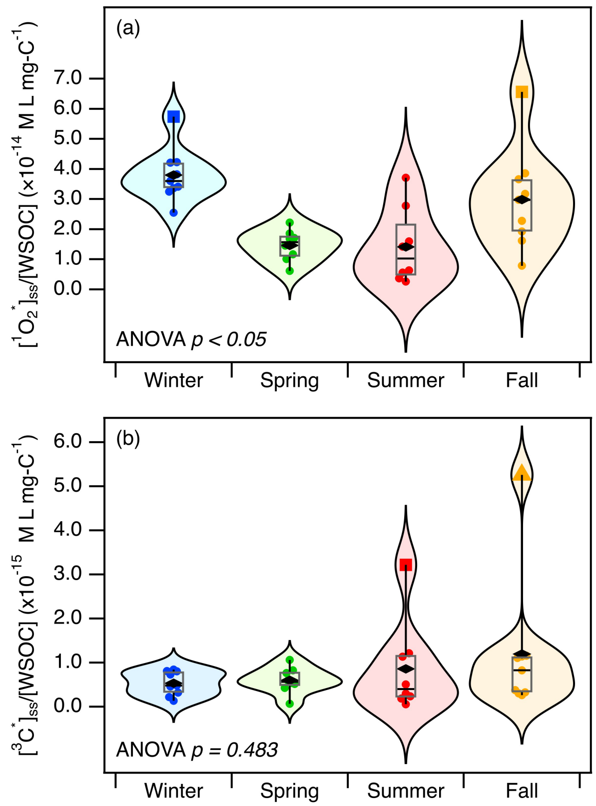

Figure S14. Violin plots showing the seasonal variations of WSOC normalized (a) $[^1O_2^*]_{ss}$ and (b) $[^3C^*]_{ss}$. For the box plots, the triangles indicate "far-out outliers" and the squares indicate outliers identified by Tukey's fences, the whiskers denote the minimum and maximum values, the boxes denote the 25th and 75th percentile values, black diamonds indicate the mean values, and the boxes' midline denote the median values.

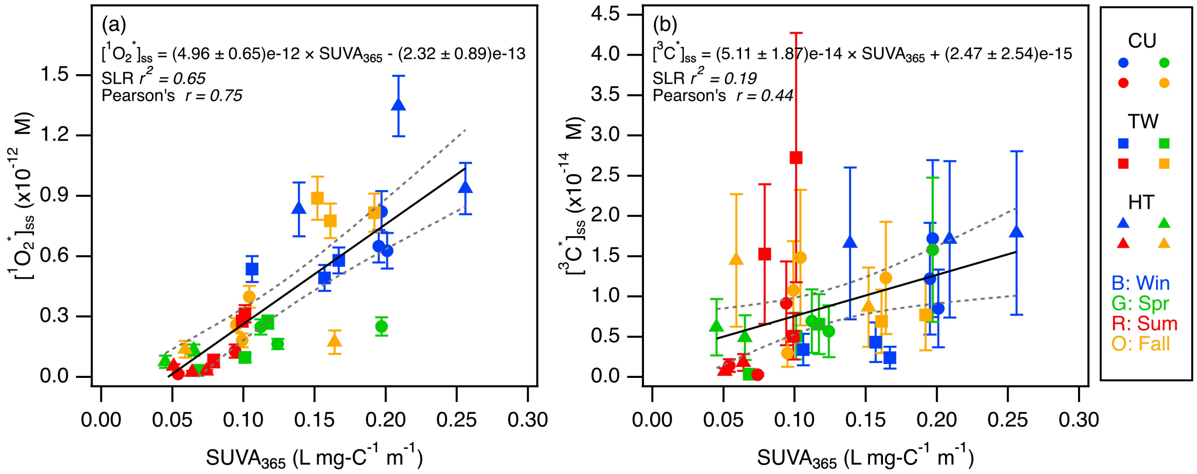

Figure S15. (a) [$^1O_2^*$]$_{ss}$ and (b) [$^3C^*$]$_{ss}$ as a function of SUVA$_{365}$. The outlier (HT271021) was excluded. Blue, green, red, and orange symbols denote the winter, spring, summer, and fall samples, respectively. Dashed lines represent 95 % confidence bands. SLR r^2 and Pearson's r are the coefficient of determination of simple linear regression and Pearson correlation coefficient, respectively.

Table S1. List of aggregated extracts for CU, TW, and HT.

Season	CityU Sample ID	CityU Total sets[a] (72 h/set)	CityU Mass ratio[b] (10^{-4})	Tsuen Wan Sample ID	Tsuen Wan Total sets[a] (72 h/set)	Tsuen Wan Mass ratio[b] (10^{-5})	Hok Tsui Sample ID	Hok Tsui Total sets[a] (72 h/set)	Hok Tsui Mass ratio[b] (10^{-4})
Winter	CU041220	3	2.11	TW110221	3	1.43	HT050121	3	1.67
	CU131220	3	1.36	TW200221	2	1.46	HT140121	3	2.01
	CU221220	2	1.68	TW260221	2	1.16	HT230121	3	1.47
Spring	CU110321	3	1.33	TW190521	3	0.49	HT090421	3	0.95
	CU200321	3	1.58	TW280521	3	0.71	HT270421	2	0.84
	CU290321	3	1.01	TW060621	3	0.91	N.A.		
Summer	CU240621	3	0.82	TW160721	3	0.86	HT130821	3	0.22
	CU030721	3	0.58	TW250721	3	1.08	HT220821	3	0.19
	N.A.			TW030821	3	1.12	HT310821	3	1.87
Fall	CU100921	2	0.87	TW161121	3	1.71	HT181021	3	0.62
	CU160921	2	0.98	TW251121	3	1.24	HT271021	3	1.14
	CU250921	3	1.48	TW061221	3	2.14	HT051121	3	0.69

Note: Due to sampler pump malfunction, filters were not collected at the CU site from 18 June 2020 to 24 June 2020 and at the HT site from 18 April 2020 to 27 April 2020.

a. Each sample set was collected continuously for 72 hours. For sample IDs that were comprised of three sets of filters (e.g., CU041220), this meant that the aggregated extracts were comprised of three consecutive 72-h sampling periods (9 days in total). For sample IDs that were comprised of two sets of filters (e.g., CU100921), this meant that the aggregated extracts were comprised of two consecutive 72-h sampling periods (6 days in total).

b. The $PM_{2.5}$ mass/water mass ratio (μg $PM_{2.5}$/μg H_2O) was calculated by taking the ratio of the $PM_{2.5}$ mass divided by the water mass for each aggregated extract sample. The $PM_{2.5}$ mass was calculated using the daily $PM_{2.5}$ mass concentration measured at or near the sampling sites by Hong Kong Environmental Protection Department (HKEPD) (https://cd.epic.epd.gov.hk/EPICDI/air/station/?lang=en). Since the CityU sampling site did not have a $PM_{2.5}$ mass monitor, the $PM_{2.5}$ mass concentration data at the closest HKEPD monitor site (Sham Shui Po, 1.5 km from CityU) was used to calculate the mass ratio for CityU samples. The $PM_{2.5}$ mass concentration data for Hok Tsui was not publicly available, and had to be requested from the HKEPD. Since a consistent extraction protocol and constant dilution ratio were applied to each aggregated sample, the $PM_{2.5}$ mass to water mass ratios were calculated on a per filter basis. To obtain the $PM_{2.5}$ mass collected onto each filter, the 9-day or 6-day averaged $PM_{2.5}$ mass concentration was multiplied by the filter sampler's flow rate (we used 29 L min^{-1} in our calculations since the sampling flow rate decreased from of 30 L min^{-1} to 28 L min^{-1} over the 72-h continuous sampling period) and sampling time (72-h $\times$ 60 min). The mass ratios were calculated under the same conditions as in photochemical experiments (i.e., measurement of $^1O_2^*$ and $^3C^*$), which was equivalent to extracting each filter in 15.54 mL Milli-Q water. These values served as an upper bound due to materials lost during water extraction and filtration process.

Table S2. Concentrations of WSOC and inorganic ions in the extracts. The values were converted to mass concentrations in air (µg m^{-3}).

Sample ID	[WSOC][a] mg-C L^{-1}	[WSOC] µg m^{-3}	[Na^+] µg m^{-3}	[NH_4^+] µg m^{-3}	[K^+] µg m^{-3}	[Mg^{2+}] µg m^{-3}	[Ca^{2+}] µg m^{-3}	[F^-] µg m^{-3}	[Cl^-] µg m^{-3}	[NO_3^-] µg m^{-3}	[SO_4^{2-}] µg m^{-3}
CU041220	21.484	2.665	0.166	1.525	2.169	0.036	0.543	0.024	1.452	2.112	5.428
CU131220	25.461	3.158	0.411	0.943	1.791	0.021	0.376	0	2.326	1.477	3.415
CU221220	18.626	2.310	0.459	1.083	1.467	0.054	0.477	0.027	1.028	1.908	4.003
CU110321	9.585	1.189	0.484	0.795	N.A.	0	0.117	0.016	N.A.	0.491	3.286
CU200321	14.895	1.848	0.474	0.966	N.A.	0.036	0.444	0.016	N.A.	0.888	4.492
CU290321	13.386	1.660	0.391	1.032	3.881	0.001	0.147	0	2.971	0.362	4.306
CU240621	8.064	1.000	0.510	0.229	3.986	0.060	0.221	0.026	3.073	0.250	2.076
CU030721	6.030	0.748	0.420	0.191	2.530	0.048	0.188	0	0.201	0.279	1.209
CU100921	11.366	1.410	0.242	0.522	5.024	0.002	0.169	0.052	3.941	0.237	2.174
CU160921	9.447	1.172	0.206	0.498	2.545	0.296	0.122	0.036	1.897	0.124	2.016
CU250921	13.395	1.662	0.434	1.409	2.078	0.047	0.140	0.013	1.533	0.263	6.047
TW110221	17.848	2.214	0.244	0.833	4.371	0.090	0.177	0.050	2.577	0.740	4.082
TW200221	13.657	1.694	0.361	0.920	2.272	0.060	0.227	0	1.626	0.578	3.974
TW260221	15.711	1.949	0.407	0.776	N.A.	0.039	0.168	0.017	N.A.	0.844	2.765
TW190521	5.409	0.671	0.355	0.208	3.040	0.040	0.160	0.018	2.478	0.318	1.403
TW280521	12.255	1.520	0.335	0.404	1.909	0.001	0.275	0.040	1.420	0.248	2.066
TW060621	6.698	0.831	0.347	0.328	N.A.	0.022	0.109	0.029	N.A.	0.230	1.678
TW160721	10.005	1.241	0.246	0.463	3.440	0.002	0.159	0.029	N.A.	0.236	1.680
TW250721	12.594	1.562	0.215	0.602	1.314	0.037	0.138	0.018	0.912	0.085	2.534
TW030821	8.466	1.050	0.284	0.655	1.984	0.040	0.090	0.029	1.424	0.164	2.686
TW161121	21.204	2.630	0.262	0.970	2.072	0.045	0.279	0.024	1.425	0.809	3.621
TW251121	25.727	3.191	0.234	0.875	1.873	0.057	0.728	0.064	1.301	0.932	3.186
TW061221	23.018	2.855	0.402	1.205	2.998	0.056	0.329	0.028	2.199	1.691	4.322
HT050121	22.240	2.759	0.452	1.223	1.291	0.001	0.449	0	0.981	2.983	3.510
HT140121	23.463	2.910	0.679	1.188	1.745	0.001	0.279	0.019	1.235	2.163	4.677
HT230121	19.715	2.445	0.642	1.065	0.138	0.001	0.092	0.013	0.922	0.702	4.785
HT090421	11.494	1.426	0.469	0.870	1.401	0.001	0.084	0.035	1.072	0.254	3.971
HT270421	7.506	0.931	0.166	0.768	1.862	0.014	0.034	0.037	1.388	0.103	2.658
HT130821	3.755	0.466	0.186	0.249	2.578	0.013	0.039	0.014	1.921	0.074	1.123
HT220821	6.154	0.763	0.191	0.405	1.697	0.016	0.020	0.027	1.270	0.056	1.581
HT310821	5.228	0.649	0.178	0.209	2.819	0.014	0.031	0	2.166	0.067	1.083
HT181021	17.541	2.176	0.296	0.364	0.596	0.041	0.163	0	0.943	0.238	5.726
HT271021	15.350	1.904	0.038	1.061	1.032	0.042	0.041	0.014	0.648	0.105	4.859
HT051121	10.625	1.318	0.409	0.610	1.781	0.001	0.218	0	1.441	0.268	2.349
Average	**13.747**	**1.705**	**0.341**	**0.748**	**1.991**	**0.036**	**0.213**	**0.021**	**1.405**	**0.655**	**3.199**
STD	6.346	0.787	0.141	0.369	1.260	0.052	0.163	0.016	0.952	0.732	1.394
CU Avg	**13.794**	**1.711**	**0.381**	**0.836**	**2.316**	**0.054**	**0.268**	**0.019**	**1.675**	**0.763**	**3.496**
CU STD	5.965	0.740	0.120	0.440	1.564	0.083	0.160	0.016	1.324	0.730	1.529
TW Avg	**14.383**	**1.784**	**0.308**	**0.687**	**2.106**	**0.041**	**0.237**	**0.029**	**1.280**	**0.573**	**2.833**
TW STD	6.506	0.807	0.068	0.296	1.287	0.025	0.171	0.017	0.914	0.461	1.011
HT Avg	**13.006**	**1.613**	**0.337**	**0.729**	**1.540**	**0.013**	**0.132**	**0.014**	**1.272**	**0.638**	**3.302**
HT STD	7.049	0.874	0.209	0.381	0.783	0.015	0.135	0.014	0.448	0.991	1.638
ANOVA p =	0.880	0.880	0.468	0.624	0.014	0.159	0.119	0.096	0.096	0.830	0.515
CU Fall+Win	16.630	2.063	0.320	0.997	2.512	0.076	0.305	0.026	2.030	1.020	3.847
CU Sum	7.047	0.874	0.465	0.210	3.258	0.054	0.205	0.013	1.637	0.265	1.643
Ratio	**2.36**	**2.36**	**0.69**	**4.75**	**0.77**	**1.40**	**1.49**	**2.00**	**1.24**	**3.85**	**2.34**
TW Fall+Win	19.528	2.422	0.318	0.930	2.717	0.058	0.318	0.030	1.825	0.932	3.658
TW Sum	10.355	1.284	0.248	0.573	2.246	0.027	0.129	0.026	0.779	0.162	2.300
Ratio	**1.89**	**1.89**	**1.28**	**1.62**	**1.21**	**2.18**	**2.47**	**1.18**	**2.34**	**5.76**	**1.59**
HT Fall+Win	18.156	2.252	0.419	0.919	1.097	0.014	0.207	0.008	1.029	1.076	4.318
HT Sum	5.046	0.626	0.185	0.288	2.365	0.014	0.030	0.013	1.786	0.066	1.262
Ratio	**3.60**	**3.60**	**2.27**	**3.19**	**0.46**	**1.00**	**6.94**	**0.57**	**0.58**	**16.35**	**3.42**

Note: Concentrations were denoted as "N.A." when they could not be determined due to IC issues. One-way ANOVA test was performed on all CU, TW, and HT samples to statistically compare the difference among the three sites.

a. The WSOC concentrations were converted to the same conditions as in the photochemical experiments.

Table S3. Optical characteristics of the extracts.

Sample ID	α_{300} cm^{-1}	R_{abs}(290-600 nm) mol-photons L^{-1} s^{-1}	MAC_{300} m^2 g-C^{-1}	$SUVA_{254}$ L mg-C^{-1} m^{-1}	$SUVA_{365}$ L mg-C^{-1} m^{-1}	AAE
CU041220	0.151	4.44×10^{-6}	1.62	1.498	0.197	7.23
CU131220	0.164	5.23×10^{-6}	1.49	1.327	0.195	6.66
CU221220	0.138	3.96×10^{-6}	1.70	1.698	0.201	7.27
CU110321	0.050	1.26×10^{-6}	1.20	1.526	0.124	8.30
CU200321	0.101	3.14×10^{-6}	1.56	1.550	0.197	7.08
CU290321	0.059	1.62×10^{-6}	1.02	1.074	0.112	7.55
CU240621	0.030	0.83×10^{-6}	0.87	0.976	0.094	7.62
CU030721	0.014	0.37×10^{-6}	0.52	0.613	0.054	6.69
CU100921	0.044	1.16×10^{-6}	0.89	0.963	0.095	7.82
CU160921	0.037	1.01×10^{-6}	0.91	0.959	0.099	7.77
CU250921	0.049	1.55×10^{-6}	0.85	0.907	0.104	6.45
TW110221	0.111	3.15×10^{-6}	1.43	1.457	0.167	7.47
TW200221	0.084	2.29×10^{-6}	1.42	1.503	0.157	7.63
TW260221	0.075	1.72×10^{-6}	1.10	1.183	0.106	6.96
TW190521	0.016	0.39×10^{-6}	0.68	0.951	0.068	7.10
TW280521	0.051	1.58×10^{-6}	0.96	1.021	0.117	6.86
TW060621	0.026	0.76×10^{-6}	0.89	1.003	0.101	6.88
TW160721	0.042	1.08×10^{-6}	0.97	1.118	0.099	7.83
TW250721	0.039	1.07×10^{-6}	0.72	0.837	0.079	7.61
TW030821	0.037	0.93×10^{-6}	1.00	1.142	0.101	8.07
TW161121	0.127	3.57×10^{-6}	1.38	1.374	0.161	7.72
TW251121	0.169	5.17×10^{-6}	1.51	1.426	0.192	6.82
TW061221	0.138	3.66×10^{-6}	1.38	1.399	0.152	7.89
HT050121	0.194	5.82×10^{-6}	2.01	1.798	0.256	7.17
HT140121	0.181	4.99×10^{-6}	1.78	1.721	0.209	7.81
HT230121	0.107	2.91×10^{-6}	1.25	1.249	0.139	7.65
HT090421	0.040	0.76×10^{-6}	0.81	1.048	0.065	7.73
HT270421	0.026	0.33×10^{-6}	0.79	0.999	0.045	8.56
HT130821	0.010	0.20×10^{-6}	0.64	0.854	0.051	7.27
HT220821	0.013	0.47×10^{-6}	0.49	0.578	0.064	5.31
HT310821	0.012	0.47×10^{-6}	0.51	0.604	0.074	5.41
HT181021	0.042	1.13×10^{-6}	0.55	0.597	0.059	7.61
HT271021	0.070	2.06×10^{-6}	1.05	1.104	0.121	6.78
HT051121	0.067	1.85×10^{-6}	1.45	1.409	0.164	7.84
Average	**0.074**	$\mathbf{2.09\times10^{-6}}$	**1.10**	**1.161**	**0.124**	**7.325**
STD	0.055	1.64×10^{-6}	0.40	0.333	0.055	0.698
CU Avg	**0.076**	$\mathbf{2.23\times10^{-6}}$	**1.15**	**1.190**	**0.134**	**7.38**
CU STD	0.053	1.66×10^{-6}	0.39	0.345	0.053	0.56
TW Avg	**0.076**	$\mathbf{2.11\times10^{-6}}$	**1.12**	**1.201**	**0.125**	**7.40**
TW STD	0.050	1.47×10^{-6}	0.29	0.224	0.039	0.45
HT Avg	**0.069**	$\mathbf{1.91\times10^{-6}}$	**1.03**	**1.087**	**0.113**	**7.20**
HT STD	0.065	1.93×10^{-6}	0.53	0.428	0.071	1.01
ANOVA p =	0.946	0.902	0.778	0.685	0.691	0.784
CU Fall+Win	0.097	2.89	1.24	1.225	0.149	7.20
CU Sum	0.022	0.60	0.70	0.795	0.074	7.62
Ratio	**4.40**	**4.83**	**1.78**	**1.54**	**2.00**	**0.94**
TW Fall+Win	0.117	3.26	1.37	1.390	0.156	7.42
TW Sum	0.039	1.02	0.90	1.032	0.093	7.84
Ratio	**2.97**	**3.19**	**1.53**	**1.35**	**1.67**	**0.95**
HT Fall+Win	0.110	3.13	1.35	1.313	0.158	7.48
HT Sum	0.012	0.38	0.55	0.679	0.063	6.00
Ratio	**9.40**	**8.19**	**2.46**	**1.93**	**2.51**	**1.25**

Note: Calculation of these light absorption properties were described in Section 2.2 in main text. One-way ANOVA test was performed on all CU, TW, and HT samples to statistically compare the difference among the three sites.

Table S4. Second order rate constants of SYR with the four model triplets used for calculations of $[^3C^*]_{ss}$.

Model $^3C^*$	Precursor	$k_{rxn}^{SYR+model\,^3C^*}$ (M^{-1} s^{-1})	Reference
$^32AN^*$	2-acetonaphthone (2AN)	$(1.9\pm0.1)\times10^9$	Kaur and Anastasio (2018)
$^33MAP^*$	3′-methoxyacetophenone (3MAP)	$(3.8\pm0.6)\times10^9$	Kaur and Anastasio (2018)
$^3DMB^*$	3,4-dimethoxybenzaldehdye (DMB)	$(3.5\pm0.8)\times10^9$	Smith et al. (2015)
$^3BP^*$	benzophenone (BP)	$(8.5\pm1.6)\times10^9$	Kaur and Anastasio (2018)

Table S5. Summary of $^{1}O_2^*$ measurements.

Sample ID	$[^{1}O_2^*]_{ss}$ [a] $\times 10^{-13}$ M	$R_{f,^{1}O_2^*}$ [b] $\times 10^{-7}$ M s^{-1}	$\Phi_{^{1}O_2^*}$ [c] %
CU041220	8.21 ± 1.02	2.31 ± 0.15	5.20 ± 0.62
CU131220	6.50 ± 0.81	1.83 ± 0.07	3.49 ± 0.37
CU221220	6.27 ± 0.89	1.76 ± 0.13	4.45 ± 0.56
CU110321	1.64 ± 0.25	0.46 ± 0.03	3.68 ± 0.46
CU200321	2.51 ± 0.46	0.70 ± 0.06	2.24 ± 0.30
CU290321	2.49 ± 0.38	0.70 ± 0.05	4.31 ± 0.53
CU240621	1.28 ± 0.33	0.36 ± 0.05	4.34 ± 0.76
CU030721	0.16 ± 0.06	0.04 ± 0.01	1.19 ± 0.31
CU100921	2.59 ± 0.34	0.73 ± 0.05	6.29 ± 0.78
CU160921	1.82 ± 0.34	0.51 ± 0.04	5.05 ± 0.66
CU250921	3.98 ± 0.55	1.12 ± 0.08	7.21 ± 0.88
TW110221	5.80 ± 0.65	1.63 ± 0.08	5.18 ± 0.57
TW200221	4.92 ± 0.65	1.38 ± 0.08	6.03 ± 0.69
TW260221	5.37 ± 0.65	1.51 ± 0.09	8.78 ± 1.03
TW190521	0.33 ± 0.08	0.09 ± 0.01	2.41 ± 0.40
TW280521	2.73 ± 0.33	0.77 ± 0.04	4.85 ± 0.56
TW060621	0.98 ± 0.21	0.27 ± 0.03	3.63 ± 0.50
TW160721	2.78 ± 0.28	0.78 ± 0.04	7.27 ± 0.80
TW250721	0.80 ± 0.32	0.22 ± 0.03	2.11 ± 0.36
TW030821	3.14 ± 0.43	0.88 ± 0.06	9.54 ± 1.18
TW161121	7.76 ± 0.86	2.18 ± 0.10	6.11 ± 0.67
TW251121	8.17 ± 0.95	2.30 ± 0.10	4.44 ± 0.49
TW061221	8.88 ± 1.07	2.50 ± 0.13	6.83 ± 0.77
HT050121	9.37 ± 1.27	2.63 ± 0.18	4.53 ± 0.54
HT140121	13.47 ± 1.50	3.79 ± 0.21	7.59 ± 0.87
HT230121	8.33 ± 1.34	2.34 ± 0.25	8.03 ± 1.19
HT090421	1.34 ± 0.28	0.38 ± 0.05	4.97 ± 0.83
HT270421	0.76 ± 0.30	0.21 ± 0.05	6.47 ± 1.51
HT130821	0.53 ± 0.10	0.15 ± 0.02	7.35 ± 1.27
HT220821	0.23 ± 0.07	0.06 ± 0.01	1.35 ± 0.33
HT310821	0.29 ± 0.06	0.08 ± 0.01	1.76 ± 0.30
HT181021	1.38 ± 0.42	0.39 ± 0.04	3.43 ± 0.49
HT271021	10.08 ± 1.42	2.83 ± 0.24	13.74 ± 1.79
HT051121	1.72 ± 0.58	0.48 ± 0.10	2.62 ± 0.59
Average	**4.02 ± 3.52**	**1.13 ± 0.99**	**5.19 ± 2.63**
CU Average	3.41 ± 2.54	0.96 ± 0.71	4.31 ± 1.70
TW Average	4.30 ± 2.97	1.21 ± 0.83	5.60 ± 2.31
HT Average	4.32 ± 4.93	1.21 ± 1.38	5.62 ± 3.58
ANOVA p =	0.792	0.792	0.417
CU Fall+Win	4.90 ± 2.49	1.38 ± 0.70	5.28 ± 1.32
CU Sum	0.72 ± 0.80	0.20 ± 0.22	2.77 ± 2.23
Ratio	**6.80**	**6.80**	**1.91**
TW Fall+Win	6.82 ± 1.66	1.92 ± 0.47	6.23 ± 1.50
TW Sum	2.24 ± 1.26	0.63 ± 0.35	6.30 ± 3.81
Ratio	**3.04**	**3.04**	**0.99**
HT Fall+Win*	6.85 ± 5.21	1.93 ± 1.46	5.24 ± 2.45
HT Sum	0.35 ± 0.16	0.10 ± 0.05	3.49 ± 3.35
Ratio*	**19.51**	**19.51**	**1.50**

Uncertainties are errors propagated from triplicate measurement of FFA loss, $^{1}O_2^*$ deactivation rates, and second-order rate constants, and/or one standard deviation from averaging. One-way ANOVA test was performed on all CU, TW, and HT samples to statistically compare the difference among the three sites.

a. Steady-state concentrations of $^{1}O_2^*$ calculated using Eq.5 in main text.

b. Formation rates of $^{1}O_2^*$ calculated using Eq.6 in main text.

c. Apparent quantum yields of $^{1}O_2^*$, calculated as the ratio of $R_{f,^{1}O_2}$ and R_{abs} (Eq.7 in main text).

* The outlier, HT271021, identified by Tukey's fences were excluded for HT Fall+Win vs. HT Sum comparisons.

Table S6. Summary of $^3C^*$ measurements.

Sample ID	k'_{SYR} [a] $\times10^{-5}$ s^{-1}	$[^32AN^*]_{ss}$ [b] $\times10^{-15}$ M	$[^33MAP^*]_{ss}$ [c] $\times10^{-15}$ M	$[^3DMB^*]_{ss}$ [d] $\times10^{-15}$ M	$[^3BP^*]_{ss}$ [e] $\times10^{-15}$ M	$[^3C^*]_{ss}$ [f] $\times10^{-15}$ M	$R_{f,^3C^*}$ [g] $\times10^{-9}$ M s^{-1}	$\Phi_{^3C^*}$ [h] %
CU041220	8.98±0.25	30.33±4.34	15.17±4.29	16.47±6.46	6.78±2.23	17.19±9.76	1.50±0.88	0.34±0.20
CU131220	6.70±0.29	21.58±3.48	10.79±3.28	11.72±4.89	4.82±1.70	12.23±6.94	1.11±0.65	0.21±0.13
CU221220	5.37±0.19	15.02±3.12	7.51±2.77	8.16±4.08	3.36±1.42	8.51±4.83	0.73±0.42	0.18±0.11
CU110321	2.76±0.02	10.04±1.03	5.02±1.22	5.45±1.89	2.24±0.65	5.69±3.23	0.45±0.26	0.35±0.21
CU200321	6.46±0.19	27.88±2.30	13.94±2.81	15.14±4.33	6.23±1.48	15.80±8.97	1.30±0.76	0.41±0.25
CU290321	3.48±0.03	12.23±1.40	6.12±1.58	6.64±2.41	2.73±0.83	6.93±3.94	0.56±0.33	0.35±0.21
CU240621	3.80±0.05	16.17±1.25	8.09±1.63	8.78±2.53	3.61±0.86	9.16±5.20	0.71±0.41	0.85±0.50
CU030721	0.79±0.01	2.49±0.27	1.24±0.35	1.35±0.55	0.56±0.19	1.41±0.80	0.11±0.06	0.29±0.17
CU100921	2.19±0.04	5.25±1.23	2.62±1.12	2.85±1.66	1.17±0.58	2.97±1.69	0.24±0.14	0.20±0.12
CU160921	4.53±0.10	19.02±1.55	9.51±1.96	10.32±3.03	4.25±1.03	10.78±6.12	0.84±0.49	0.83±0.49
CU250921	6.67±0.25	26.17±2.78	13.08±3.01	14.21±4.59	5.85±1.58	14.83±8.42	1.20±0.70	0.78±0.46
TW110221	3.16±0.06	4.26±2.46	2.13±1.93	2.3±2.76	0.95±0.98	2.41±1.37	0.20±0.12	0.06±0.04
TW200221	3.48±0.09	7.64±2.22	3.82±0.89	4.15±2.77	1.71±0.97	4.33±2.46	0.35±0.21	0.15±0.09
TW260221	3.34±0.08	6.04±2.37	3.02±1.92	3.28±2.78	1.35±0.98	3.42±1.94	0.28±0.17	0.17±0.10
TW190521	0.50±0.01	0.61±0.24	0.31±0.26	0.33±0.39	0.14±0.13	0.35±0.20	0.03±0.02	0.07±0.04
TW280521	3.44±0.07	11.58±1.49	5.79±1.59	6.29±2.42	2.59±0.83	6.56±3.73	0.53±0.31	0.33±0.20
TW060621	2.32±0.05	8.98±0.82	4.49±1.01	4.88±1.57	2.01±0.53	5.09±2.89	0.39±0.23	0.51±0.30
TW160721	2.96±0.06	8.93±1.41	4.46±1.42	4.85±2.13	2.00±0.74	5.06±2.87	0.40±0.23	0.37±0.22
TW250721	5.67±0.20	26.94±1.92	13.47±2.42	14.63±3.76	6.02±1.28	15.27±8.67	1.23±0.72	1.15±0.69
TW030821	10.54±0.29	48.12±3.53	24.06±4.51	26.12±7.00	10.76±2.39	27.27±15.48	2.11±1.23	2.28±1.35
TW161121	5.38±0.11	12.22±3.44	6.11±2.93	6.63±4.28	2.73±1.50	6.92±3.93	0.60±0.35	0.17±0.10
TW251121	5.79±0.10	13.61±3.62	6.81±3.12	7.39±4.57	3.04±1.60	7.71±4.38	0.70±0.41	0.14±0.08
TW061221	6.37±0.13	15.32±3.98	7.66±3.43	8.32±5.02	3.42±1.76	8.68±4.93	0.77±0.45	0.21±0.12
HT050121	9.64±0.33	31.59±4.93	15.80±4.70	17.15±7.02	7.06±2.43	17.90±10.16	1.58±0.92	0.27±0.16
HT140121	10.85±0.41	30.21±6.51	15.10±5.68	16.40±8.34	6.75±2.92	17.12±9.72	1.52±0.89	0.31±0.18
HT230121	8.82±0.31	29.28±4.66	14.64±4.33	15.89±6.44	6.54±2.24	16.59±9.42	1.43±0.84	0.49±0.29
HT090421	2.39±0.10	8.64±1.04	4.32±1.09	4.69±1.65	1.93±0.57	4.90±2.78	0.39±0.23	0.52±0.31
HT270421	2.61±0.07	10.94±0.91	5.47±1.13	5.94±1.75	2.44±0.60	6.20±3.52	0.47±0.28	1.44±0.85
HT130821	0.69±0.02	1.22±0.34	0.61±0.34	0.66±0.52	0.27±0.18	0.69±0.39	0.05±0.03	0.25±0.15
HT220821	0.95±0.02	3.20±0.34	1.60±0.42	1.74±0.66	0.72±0.22	1.81±1.03	0.14±0.08	0.29±0.17
HT310821	0.47±0.01	0.52±0.22	0.26±0.24	0.28±0.37	0.12±0.13	0.29±0.17	0.02±0.01	0.05±0.03
HT181021	5.62±0.19	25.59±1.96	12.79±2.42	13.89±3.74	5.72±1.28	14.50±8.23	1.22±0.72	1.08±0.64
HT271021	30.98±2.19	142.56±14.96	71.28±14.33	77.39±21.42	31.87±7.43	80.77±45.86	6.68±3.91	3.24±1.92
HT051121	5.01±0.05	21.72±1.69	10.86±2.15	11.79±3.34	4.86±1.14	12.31±6.99	0.97±0.57	0.53±0.31
Average	5.37±5.35	19.29±24.48	9.65±12.24	10.47±13.29	4.31±5.47	10.93±13.87	9.07±11.50	0.56±0.66
CU Avg	4.70±2.40	16.93±9.11	8.46±4.55	9.19±4.94	3.78±2.04	9.59±5.16	7.95±4.47	0.44±0.26
TW Avg	4.41±2.56	13.69±12.69	6.84±6.34	7.43±6.89	3.06±2.84	7.76±7.19	6.33±5.60	0.47±0.65
HT Avg	7.09±8.75	27.77±39.39	13.88±19.96	15.07±21.67	6.21±8.93	15.73±22.26	13.17±18.78	0.77±0.91
ANOVA p =	0.441	0.370	0.370	0.370	0.370	0.370	0.34	0.435
CU Fall+Win	5.74±2.30	19.56±8.83	9.78±4.41	10.62±4.79	4.37±1.97	11.08±5.00	9.37±4.39	0.42±0.30
CU Sum	2.29±2.13	9.33±9.67	4.67±4.84	5.06±5.25	2.09±2.16	5.29±5.48	4.06±4.24	0.57±0.40
Ratio	**2.50**	**2.10**	**2.10**	**2.10**	**2.10**	**2.10**	**2.30**	**0.74**
TW Fall+Win	4.59±1.42	9.85±4.48	4.92±2.24	5.35±2.43	2.20±1.00	5.58±2.54	4.86±2.36	0.15±0.05
TW Sum	6.39±3.84	28.00±19.62	14.00±9.81	15.20±10.65	6.29±4.39	15.86±11.12	12.46±8.57	1.27±0.96
Ratio*	**0.72**	**0.35**	**0.35**	**0.35**	**0.35**	**0.35**	**0.39**	**0.12**
HT Fall+Win*	7.99±2.55	27.68±4.00	13.84±2.00	15.02±2.17	6.19±0.90	15.68±2.27	13.45±2.48	0.54±0.33
HT Sum	0.70±0.24	1.65±1.39	0.82±0.70	0.89±0.75	0.37±0.31	0.93±0.79	0.70±0.60	0.20±0.13
Ratio*	**11.39**	**16.81**	**16.81**	**16.81**	**16.81**	**16.81**	**19.21**	**2.74**

Uncertainties are errors propagated from triplicate measurement of SYR loss, and second-order rate constants, and/or one standard deviation from averaging. One-way ANOVA test was performed on all CU, TW, and HT samples to statistically compare the difference among the three sites.

a. The measured pseudo first-order rate constant for SYR loss for each PM extract sample.

b to e. Estimated concentration of model $^3C^*$, 2-acetonaphthone (2AN), 3′-methoxyacetophenone (3MAP), 3,4-dimethoxybenzaldehdye (DMB), and benzophenone (BP), based on the measured k'_{SYR} and their second-order rate constants with SYR as listed in Table S4.

f. Steady-state concentrations of $^3C^*$ obtained by averaging the concentrations of four model $^3C^*$ (Eq.8 in main text).

g. Formation rates of $^3C^*$ calculated using Eq.9 in main text.

h. Apparent quantum yields of $^3C^*$, calculated as the ratio of $R_{f,^3C^*}$ and R_{abs} (Eq.10 in main text).

* The outlier, HT271021, identified by Tukey's fences were excluded for HT Fall+Win vs. HT Sum comparisons.

Table S7. Summary of $[^1O_2^*]_{ss}$ and $[^3C^*]_{ss}$ in atmospheric samples.

Sample type	$[^1O_2^*]_{ss}$ ($\times 10^{-13}$ M)		$[^3C^*]_{ss}$ ($\times 10^{-15}$ M)		Experimental condition	Reference
	Range	Average	Range	Average		
Fog water	1.1 - 6.1	2.23 ± 1.91	N.A.	N.A.	*footnote a*	Anastasio and McGregor (2001)
Fog water	0.11-3	1.67 ± 0.93	7-150	50.14 ± 51.44	*footnote b*	Kaur and Anastasio (2017, 2018)
Rain water	≤ 0.027	N.A.	N.A.	N.A.	*footnote c*	Albinet et al. (2010)
Rain water	0.30-1.51	0.99 ± 0.62	10.8-17.2	14.33 ± 3.25	*footnote d*	Hong et al. (2018)
$PM_{2.5}$ extracts	0.64-22	9.60 ± 8.05	0.51-160	67.81 ± 45.66	*footnote e*	Kaur et al. (2019)
PM_{10} extracts	0.08 & 0.14	0.11	N.A.	N.A.	*footnote f*	Manfrin et al. (2019)
$PM_{2.5}$ extracts	N.A.	N.A.	68-255	167 ± 59.17	*footnote g*	Chen et al. (2021)
$PM_{2.5}$ extracts	1.1-3.4	1.88 ± 0.77	N.A.	N.A.	*footnote h*	Leresche et al. (2021)
PM_{10} extracts	0.33-4.59	N.A.	N.A.	N.A.	*footnote i*	Bogler et al. (2022)
$PM_{2.5}$ extracts	2.1-85	35.9 ± 29.7	20-700 (SYR) 3.7-410 (PTA)	445 ± 245 221 ± 130	*footnote j*	Ma et al. (2023)
$PM_{2.5}$ extracts	0.16-13.47	4.02 ± 3.52	0.29-80.77	10.93 ± 13.87	*footnote k*	This work

Note that FFA was used as the $^1O_2^*$ probe in all cited literature while the different probes for $^3C^*$ were noted below.

a. [WSOC]: 14.4 - 45.6 mg-C L^{-1}. $[^1O_2^*]_{ss}$ were corrected using 50 % D_2O to exclude contribution of other reactive species to the observed FFA decay. The values were subsequently normalized to the values expected in midday Davis winter-solstice sunlight.

b. [WSOC]: 8.04 - 21.48 mg-C L^{-1}. $[^1O_2^*]_{ss}$ were corrected using 50 % D_2O to exclude contribution of other reactive species to the observed FFA decay. $[^3C^*]_{ss}$ were obtained using a dual-probe technique by averaging $[^3C^*]_{ss}$ measured by syringol (SYR) and methyl jasmonate (MeJA). These values were subsequently normalized to the values expected in midday Davis winter-solstice sunlight.

c. [WSOC]: 0.60 - 2.38 mg-C L^{-1}. 5 UVA lamps (Philips TL K05) with emission maximum at 365 nm and a photon flux of 57 W m^{-2} (1.6×10^{-5} Einstein L^{-1} s^{-1}), which is approximately two times that of sunny summer solar irradiance at mid-latitude (ca. 30 W m^{-2}). $[^1O_2^*]_{ss}$ for five out of six rain water samples were on the order of 10^{-21}-10^{-19} M. The other sample had a $[^1O_2^*]_{ss}$ of $(2.7 \pm 0.3) \times 10^{-15}$ M.

d. [WSOC]: 0.72 - 3.04 mg-C L^{-1}. Hg lamp and a glass cut off (λ<290 nm) with irradiance of 70.7 W m^{-2} in the range of 290-400 nm, equivalent to 1.6 sun power. $[^1O_2^*]_{ss}$ were corrected by subtracting the contribution of hydroxyl radical to the FFA decay. $[^3C^*]_{ss}$ were measured using TMP as the $^3C^*$ probe but neglecting contribution of hydroxyl radical to the TMP loss.

e. [WSOC]: 4.27 - 85.58 mg-C L^{-1}. 1000 W xenon lamp was used as the light source, equipped with a water filter (to reduce sample heating), an air mass 1.0 filter (AM1D-3L, Sciencetech), and a 295 nm long-pass fil- ter (20CGA-295, Thorlabs) . $[^1O_2^*]_{ss}$ was corrected using 50 % D_2O to exclude contribution of other reactive species to the observed FFA decay. $[^3C^*]_{ss}$ were measured and scaled using SYR and methyl jasmonate (MeJA) as the $^3C^*$ probes. The values were subsequently normalized to the values expected in midday Davis winter-solstice sunlight.

f. [WSOC] was controlled at 5 mg-C L^{-1}. SMART narrow-band hand-held lamp at 311 nm was used as the light source. $[^1O_2^*]_{ss}$ were corrected by subtracting the contribution of hydroxyl radical to the FFA decay.

g. [WSOC]: 24.01 - 41.87 mg-C L^{-1}. Xenon lamp with a VISREF filter (PLS-SXE 300, Perfectlight), approximately 1.2-1.3 times that of noon sunlight. 4 mM TMP was used as the triplet probe and only the observed pseudo first-order rates were reported. The $[^3C^*]_{ss}$ in the table represent upper limits that were estimated by dividing the reported TMP loss rates by the second-order rate constant of TMP with model triplets (3.0×10^9 M^{-1} s^{-1}, (al Housari et al., 2010)).

h. 1000 W xenon lamp and an air mass 1.5 filter was used as the light source. $[^1O_2^*]_{ss}$ were corrected by adding 0.1 M methanol as hydroxyl radical quencher and were normalized to [WSOC] of 11.5 mg-C L^{-1}.

i. [WSOC] were not available. 12 UVA broad band lamps (RPR-3500Å, Southern New England Ultraviolet Co.) with emission centered at 365 nm was used as the light source. The average absolute irradiance of the light source is 221.18 ± 43.92 W m^{-2}. $[^1O_2^*]_{ss}$ was corrected by adding 100 μM *iso*-propynol as hydroxyl radical quencher.

j. [WSOC]: 10.1 - 495.4 mg-C L^{-1}. 1000 W xenon lamp was used as the light source, equipped with a water filter (to reduce sample heating), an air mass 1.0 filter (AM1D-3L, Sciencetech), and a 295 nm long-pass fil- ter (20CGA-295, Thorlabs) . $[^1O_2^*]_{ss}$ was corrected using 50 % D_2O to exclude contribution of other reactive species to the observed FFA decay. $[^3C^*]_{ss}$ were measured using (phenythio)acetic acid (PTA) and SYR as the $^3C^*$ probes, respectively. The values were subsequently normalized to the values expected in midday Davis winter-solstice sunlight.

k. [WSOC]: 3.76 - 25.73 mg-C L^{-1}. 12 UVA broad band lamps (RPR-3500Å, Southern New England Ultraviolet Co.) with emission centered at 365 nm was used as the light source. The photon flux of the light source was higher than solar irradiance on summer solstice at noon (Figure S5). $[^1O_2^*]_{ss}$ was corrected by using 50 % D_2O to exclude contribution of other reactive species to the observed FFA decay. $[^3C^*]_{ss}$ were measured using SYR as the $^3C^*$ probe but neglecting contribution of hydroxyl radical to the SYR loss.

Table S8. Results of t-tests performed on pairs of seasonal values for $PM_{2.5}$ mass/H_2O mass ratio, WSOC concentration, light absorption properties of water-soluble BrC, and $[^1O_2^*]_{ss}$.

$PM_{2.5}$ mass/H_2O mass	Winter	Spring	Summer	Fall
Winter	/	Statistically significant	Statistically significant	N.S.
Spring	Statistically significant	/	N.S.	N.S.
Summer	Statistically significant	N.S.	/	Statistically significant
Fall	N.S.	N.S.	Statistically significant	/

[WSOC], $[^1O_2^*]_{ss}$	Winter	Spring	Summer	Fall
Winter	/	Statistically significant	Statistically significant	N.S.
Spring	Statistically significant	/	N.S.	Statistically significant
Summer	Statistically significant	N.S.	/	Statistically significant
Fall	N.S.	Statistically significant	Statistically significant	/

α_{300}, **R_{abs}**, **$SUVA_{365}$**	Winter	Spring	Summer	Fall
Winter	/	Statistically significant	Statistically significant	Statistically significant
Spring	Statistically significant	/	N.S.	N.S.
Summer	Statistically significant	N.S.	/	Statistically significant
Fall	Statistically significant	N.S.	Statistically significant	/

MAC_{300}, $SUVA_{254}$	Winter	Spring	Summer	Fall
Winter	/	Statistically significant	Statistically significant	Statistically significant
Spring	Statistically significant	/	Statistically significant	N.S.
Summer	Statistically significant	Statistically significant	/	Statistically significant
Fall	Statistically significant	N.S.	Statistically significant	/

Note: The student's t-test was used to determine whether the difference in the parameters between two seasons was statistically significant. The difference was statistically significant when $p < 0.05$. Conversely, the difference was not statistically significant (denoted as "N.S.") when $p > 0.05$. Only the parameters that were shown to be statistically significant in one-way ANOVA analysis are shown in this table. While not shown in this table, the student's t tests showed that the differences in the $[^3C^*]_{ss}$, $\Phi_{^3C^*}$, and $\Phi_{^1O_2^*}$ values between the different seasons were not statistically significant. Only the seasonal values for the $PM_{2.5}$ mass/H_2O mass ratio and WSOC concentration matched (or had somewhat close) trends as the seasonal $[^1O_2]_{ss}$ values with regards to whether the difference in the parameters between two seasons was statistically significant. This suggested that the observed seasonal differences in the $[^1O_2]_{ss}$ values were driven primarily by the $PM_{2.5}$ mass concentration and WSOC concentration.

References

al Housari, F., Vione, D., Chiron, S., and Barbati, S.: Reactive photoinduced species in estuarine waters. Characterization of hydroxyl radical, singlet oxygen and dissolved organic matter triplet state in natural oxidation processes, Photochemical & Photobiological Sciences, 9, 78–86, https://doi.org/https://doi.org/10.1039/B9PP00030E, 2010.

Albinet, A., Minero, C., and Vione, D.: Photochemical generation of reactive species upon irradiation of rainwater: Negligible photoactivity of dissolved organic matter, Science of the total environment, 408, 3367–3373, 2010.

Anastasio, C. and McGregor, K. G.: Chemistry of fog waters in California's Central Valley: 1. In situ photoformation of hydroxyl radical and singlet molecular oxygen, Atmospheric Environment, 35, 1079–1089, 2001.

Bogler, S., Daellenbach, K. R., Bell, D. M., Prévôt, A. S., El Haddad, I., and Borduas-Dedekind, N.: Singlet Oxygen Seasonality in Aqueous PM10 is Driven by Biomass Burning and Anthropogenic Secondary Organic Aerosol, Environmental Science & Technology, 56, 15 389–15 397, https://doi.org/10.1021/acs.est.2c04554, 2022.

Chen, Q., Mu, Z., Xu, L., Wang, M., Wang, J., Shan, M., Fan, X., Song, J., Wang, Y., Lin, P., et al.: Triplet-state organic matter in atmospheric aerosols: Formation characteristics and potential effects on aerosol aging, Atmospheric Environment, 252, 118 343, https://doi.org/10.1016/j.atmosenv.2021.118343, 2021.

Galbavy, E. S., Ram, K., and Anastasio, C.: 2-Nitrobenzaldehyde as a chemical actinometer for solution and ice photochemistry, Journal of Photochemistry and Photobiology A: Chemistry, 209, 186–192, https://doi.org/10.1016/j.jphotochem.2009.11.013, 2010.

Hong, J., Liu, J., Wang, L., Kong, S., Tong, C., Qin, J., Chen, L., Sui, Y., and Li, B.: Characterization of reactive photoinduced species in rainwater, Environmental Science and Pollution Research, 25, 36 368–36 380, https://doi.org/10.1007/s11356-018-3499-4, 2018.

Kaur, R. and Anastasio, C.: Light absorption and the photoformation of hydroxyl radical and singlet oxygen in fog waters, Atmospheric Environment, 164, 387–397, https://doi.org/10.1016/j.atmosenv.2017.06.006, 2017.

Kaur, R. and Anastasio, C.: First measurements of organic triplet excited states in atmospheric waters, Environmental science & technology, 52, 5218–5226, https://doi.org/10.1021/acs.est.7b06699, 2018.

Kaur, R., Labins, J. R., Helbock, S. S., Jiang, W., Bein, K. J., Zhang, Q., and Anastasio, C.: Photooxidants from brown carbon and other chromophores in illuminated particle extracts, Atmospheric Chemistry and Physics, 19, 6579–6594, https://doi.org/10.5194/acp-19-6579-2019, 2019.

Leresche, F., Salazar, J. R., Pfotenhauer, D. J., Hannigan, M. P., Majestic, B. J., and Rosario-Ortiz, F. L.: Photochemical aging of atmospheric particulate matter in the aqueous phase, Environmental Science & Technology, 55, 13 152–13 163, https://doi.org/10.1021/acs.est.1c00978, 2021.

Ma, L., Worland, R., Jiang, W., Niedek, C., Guzman, C., Bein, K. J., Zhang, Q., and Anastasio, C.: Predicting photooxidant concentrations in aerosol liquid water based on laboratory extracts of ambient particles, EGUsphere, 2023, 1–36, https://doi.org/10.5194/egusphere-2023-566, 2023.

Manfrin, A., Nizkorodov, S. A., Malecha, K. T., Getzinger, G. J., McNeill, K., and Borduas-Dedekind, N.: Reactive oxygen species production from secondary organic aerosols: the importance of singlet oxygen, Environmental Science & Technology, 53, 8553–8562, https://doi.org/10.1021/acs.est.9b01609, 2019.

Smith, J. D., Kinney, H., and Anastasio, C.: Aqueous benzene-diols react with an organic triplet excited state and hydroxyl radical to form secondary organic aerosol, Phys. Chem. Chem. Phys., 17, 10 227–10 237, https://doi.org/10.1039/C4CP06095D, 2015.